Robotica: (2021) volume 39, pp. 2079–2093. © The Author(s), 2021. Published by Cambridge University Press.
doi:10.1017/S0263574721000151

Fatigue Life and Reliability Analysis of a Parallel Hip Joint Simulator

Feng Guo†, Gang Cheng†‡* and Xin Yuan†

† *School of Mechatronic Engineering, China University of Mining and Technology, Xuzhou, China*
E-mails: guofengcumt@163.com, yxincmee@163.com
‡ *Executive director, Shandong Zhongheng Optoelectronic Technology Co., Ltd., Zaozhuang, China*

(Accepted January 19, 2021. First published online: February 22, 2021)

SUMMARY
Aiming at 3SPS+1PS parallel hip joint simulator, the maximum stress of branched chains under the suggested trajectory is obtained by elastodynamic analysis. Based on Corten-Dolan fatigue damage theory and Rain-flow counting method, the dynamic stress of each branched chain is statistically analyzed. The fatigue life prediction shows that branched-chain $A_2P_2C_2$ is the weakest component for the simulator. Finally, the fatigue reliability is analyzed and the fatigue life and reliability under different structural parameters are discussed. The study shows that the fatigue life of each branched chain can be increased or balanced by increasing structural parameters or exchanging initial motion parameters.

KEYWORDS: Parallel simulator elastodynamics; Corten-Dolan fatigue damage theory; Rain-flow counting method; Fatigue life; Fatigue reliability.

1. Introduction

Compared with series manipulators, parallel manipulators with a high speed, low weight, and high precision have gained intensive attention in the research field of mechanism.[1–3] At present, most of the research on parallel manipulators focuses on kinematics and dynamic analysis,[4,5] performance analysis,[6,7] error compensation,[8,9] and so on. When a manipulator operates at a high speed, a series of low-order resonances occur, resulting in periodic changes in the dynamic stress on the robots that cause strength failure and fatigue damage. Fatigue and strength failures being the main forms of failure, fatigue analysis of a manipulator provides the foundation for its structural optimization and life prediction.

Fatigue life is defined as the frequency or time until the manipulator components are destroyed under cyclic load. The fatigue life is divided into two parts: crack initiation time and crack propagation time. At present, the research concerning the fatigue life prediction of the mechanisms is limited. Examples of fatigue life prediction methods include the nominal stress method, strain method, and energy method. Sun et al. used the obtained load history data and bending stress results, the big modulus gear's fatigue life was predicted based on the nominal stress method.[10] Nie et al. analyzed the stress variations caused by the robot operating at different poses using different rivets, presented a method for modeling and analyzing the fatigue life of robots with flexible joints under percussive impact forces.[11] Guo et al. analyzed the fatigue life, damage, safety, and fatigue sensitivity, and the weak areas for an amphibious spherical robot with FEA.[12] Liu et al. simulated the dangerous point probability density function for the stress and strain in the structure by the FEA method and established a reliable model for two aircraft engine chassis with low-cycle fatigue lives by combining the linear fatigue damage accumulation theory.[13] Yan used the Miner cumulative damage theory to transform the complex random stress history into equivalent constant amplitude cyclic stress and

* Corresponding author. E-mail: chg@cumt.edu.cn

established the reliability model of the series system considering the statistical dependence among part failures.[14] Kassner established the fatigue assessment methods for the bogie frame of a rolling stock and showed the potential and the advantages of the fatigue assessment with the real loading assumptions and with different evaluation methods by comparing stress analyses for some selected stress points.[15] Cai et al. considered the load frequency effects in the fatigue life prediction models and proposed an extended model based on the *S-N* approach considering the frequency effect.[16] Considering a more common failure mechanism that railway contact wires are exposed to repeated mechanical strain and stress caused by their own weight and discontinuous contact, Kim et al. utilized the maximum local stress on the top of a contact wire to predict its bending fatigue life.[17] Gao et al. redefined the value of exponent d in the Corten-Dolan model to improve it, and the improved model resulted in significantly smaller errors than the traditional model.[18] Using the power form of the stress ratio between two consecutive load levels to modify the parameter d of Corten-Dolan model, Liu et al. proposed a new improved version to reflect the nonlinear effect of load interaction and obtained more satisfactory prediction of fatigue life.[19] Cheng et al. proposed a new approach for the evaluation of Rain-flow fatigue damage to avoid the problem of transformation-based methods and provide accurate estimation for fatigue damage of narrowband leptokurtic non-Gaussian random loading.[20] Considering the dynamic load characteristics of a machining center, Chen et al. obtained the joint distribution function of the mean and amplitude of the radial force, axial force, and cutting torque and compiled the two-dimensional load spectrum of the machining center based on Rain-flow counting method.[21]

The 3SPS+1PS parallel simulator is mainly used for friction and wear tests of artificial hip joints and must run continuously and reliably for a long time. According to ISO14242-1 for the test standard of artificial hip joints, the motion period of the parallel simulator is 1s and its working frequency is 1 ± 0.1Hz. The dynamic stress of the branched chains will lead to fatigue damage for the simulator, therefore, it is necessary to analyze the fatigue life and reliability. In this paper, the unsteady, asymmetric, and variable dynamic stress amplitude of the flexible branched chains is calculated by elastodynamic analysis. The fatigue lives of branched chains are estimated based on the Corten-Dolan fatigue cumulative damage theory and the Rain-flow counting method. Based on the Monte Carlo model, the fatigue reliability of the parallel manipulator is analyzed, and the measures to improve the fatigue life and reliability of the parallel simulator are proposed.

2. Elastodynamic Model of 3SPS+1PS Parallel Simulator

The test prototype and topology structure of 3SPS+1PS parallel simulator is shown in Fig. 1(a) and (b). The parallel simulator is composed of a moving platform, a base, three SPS branched chains, and a PS branched chain. The three SPS branched chains connect the base and moving platform with a spherical joint S. One end of the branched-chain PS is fixed, and the other end is connected with the moving platform by a spherical joint S. The 3SPS+1PS parallel simulator has a translational DoF and three rotational DoF for the moving platform in the workspace. During the artificial hip joint friction test, the translational DoF of the parallel simulator is limited and used to balance the test loading force of the hydraulic system, the three rotational DoF are used to simulate the motion of the human hip joint.

The bottom of the branched-chain PS is fixed to the base at point O, and each of the four branched chains contains a moving pair P_i. The centers of all the spherical hinge on the moving platform form a regular triangle $\Delta C_1C_2C_3$ whose center is $o(C_4)$, and the centers of all the spherical hinges on the base form a regular triangle $\Delta A_1A_2A_3$ whose center is $O(A_4)$. Then, the local coordinate system o-xyz and absolute coordinate system O-XYZ are established on the moving platform center and the base center, respectively. z-axis is perpendicular to the moving platform and Z-axis is perpendicular to the base, x-axis and X-axis are parallel to C_2C_3 and A_2A_3, respectively, y-axis and Y-axis satisfy the right-hand rule. The branched-chain reference coordinate system A_i-$X_iY_iZ_i$ is established at point A_i and is parallel to the system O-XYZ. Then, the coordinate system A_i-$x_{i1}y_{i1}z_{i1}$ is established and moves with branched-chain component A_iP_i, x_{i1}-axis is parallel to X_i-axis, and z_i-axis is along the direction of A_iP_i. Similarly, the coordinate system P_i-$x_{i2}y_{i2}z_{i2}$ is established at point P_i and moves with the branched-chain component P_iC_i. The topological structure of the branched chain is shown in Fig. 1(c).

https://doi.org/10.1017/S0263574721000151 Published online by Cambridge University Press

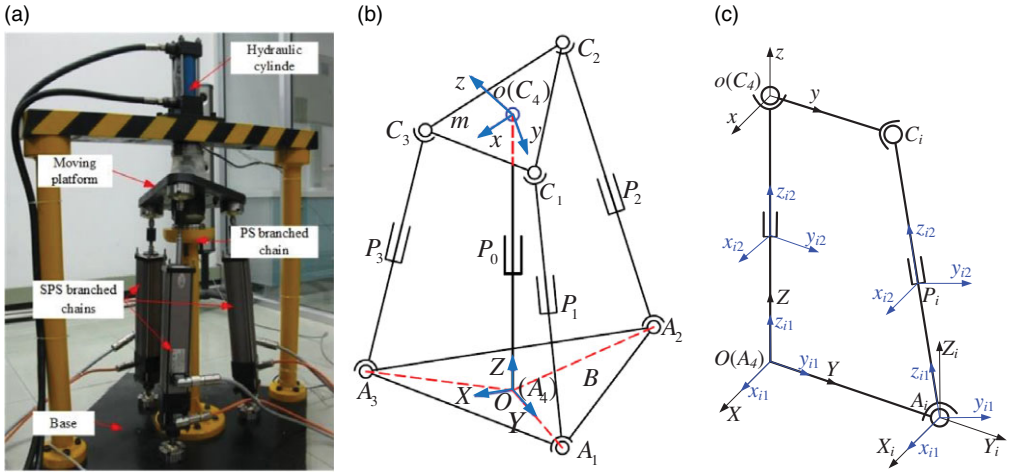

Fig. 1. 3SPS+1PS parallel hip joint simulator. (a) Test prototype. (b) Topology structure. (c) Topology structure of a branched-chain $A_i P_i C_i$.

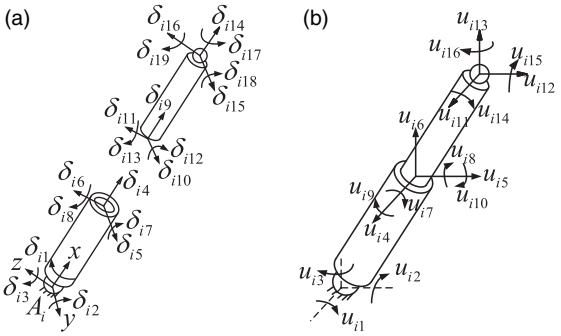

Fig. 2. Dynamic model of the branched chain. (a) Dynamic model in the element coordinate system. (b) Dynamic model in the absolute coordinate system.

For 3SPS+1PS parallel hip joint simulator, the stiffness of the moving platform, the base, and the intermediate branched-chain PS is much larger than three peripheral branched chains. It is only assumed that the branched-chain $A_iP_iC_i (i = 1, 2, 3)$ is the flexible component, and the flexibility of branched-chain joints is ignored. The elastic elements $i1$ and $i2$ ($i = 1, 2, 3$) are set on the branched-chain components A_iP_i and P_iC_i, respectively, so there are six flexible elements in total. The three peripheral branched chains of 3SPS+1PS parallel simulator have the same structural parameters. Hence, one of three branched chains $A_i P_i C_i$ is selected for elastodynamic analysis. The circular beam is chosen as the basic element, $\delta_1 \sim \delta_3$ and $\delta_{10} \sim \delta_{12}$ represent the elastic displacements of the element node, $\delta_4 \sim \delta_6$ and $\delta_{13} \sim \delta_{15}$ represent the elastic rotation angles of the element node, $\delta_7 \sim \delta_9$ and $\delta_{16} \sim \delta_{18}$ represent the elastic curvature of the element node.

According to the structural characteristics of 3SPS+1PS parallel simulator, the branched-chain component $A_i P_i$ can be treated as a cantilever beam, therefore the elastic displacement at the node A_i is zero. The node P_i is a prismatic pair and the nodes A_i and C_i are ball pairs, therefore the elastic curvature at the nodes P_i and C_i are zero. There are 8 nonzero element coordinates for the branched-chain component $A_i P_i$ and 11 nonzero element coordinates for the branched-chain component $P_i C_i$, as shown in Fig. 2(a). The node deformations of the branched-chain $A_iP_iC_i$ can be expressed by 16 absolute coordinates $\boldsymbol{U}_i = [u_{i1}, u_{i2}, \cdots, u_{i15}, u_{i16}]^{\mathrm{T}}$, as shown in Fig. 2(b).

The transformation relationship between the element coordinates of the element and the absolute coordinates for the branched-chain components A_iP_i and P_iC_i are as follows:

$$\begin{cases} \boldsymbol{\delta}_{AiPi} = \mathrm{diag}\left(\boldsymbol{R}_{i1}\ \boldsymbol{R}_{i1}\ \boldsymbol{R}_{i1}\ \boldsymbol{R}_{i1}\ \boldsymbol{R}_{i1}\ \boldsymbol{R}_{i1}\right)\boldsymbol{u}_{AiPi} \\ \boldsymbol{\delta}_{PiCi} = \mathrm{diag}\left(\boldsymbol{R}_{i1}\ \boldsymbol{R}_{i1}\ \boldsymbol{R}_{i1}\ \boldsymbol{R}_{i1}\ \boldsymbol{R}_{i1}\ \boldsymbol{R}_{i1}\right)\boldsymbol{u}_{PiCi} \end{cases}, \tag{1}$$

https://doi.org/10.1017/S0263574721000151 Published online by Cambridge University Press

where $\boldsymbol{R}_{i1}$ is the transformation matrix from the system *O-XYZ* to the system A_i-*xyz*.

$$\begin{cases} \boldsymbol{\delta}_{Ai\,Pi} = [0, 0, 0, \delta_{i1}, \delta_{i2}, \delta_{i3}, 0, 0, 0, \delta_{i4}, \delta_{i5}, \delta_{i6}, 0, \delta_{i7}, \delta_{i8}, 0, 0, 0]^{\mathrm{T}} \\ \boldsymbol{u}_{Ai\,Pi} = [0, 0, 0, u_{i1}, u_{i2}, u_{i3}, 0, 0, 0, u_{i4}, u_{i5}, u_{i6}, u_{i7}, u_{i8}, 0, 0, 0, 0]^{T} \\ \boldsymbol{\delta}_{PiCi} = [\delta_{i9}, \delta_{i10}, \delta_{i11}, 0, \delta_{i12}, \delta_{i13}, 0, 0, 0, \delta_{i14}, \delta_{i15}, \delta_{i16}, \delta_{i17}, \delta_{i18}, \delta_{i19}, 0, 0, 0]^{T} \\ \boldsymbol{u}_{PiCi} = [u_{i4}, u_{i5}, u_{i6}, u_{i9}, u_{i10}, 0, 0, 0, 0, u_{i11}, u_{i12}, u_{i13}, u_{i14}, u_{i15}, u_{i16}, 0, 0, 0]^{T} \end{cases}$$

According to the Lagrange equation and combined with Eq. (1), the dynamics model of the branched-chain $A_i P_i C_i$ can be obtained as follows:

$$\boldsymbol{M}^i \ddot{\boldsymbol{U}}_i + \boldsymbol{K}^i \boldsymbol{U}_i = \boldsymbol{F}^i + \boldsymbol{P}^i + \boldsymbol{Q}^i, \tag{2}$$

where $\boldsymbol{U}_i$ is the node absolute coordinates, $\boldsymbol{M}^i$ is the mass matrix, $\boldsymbol{k}^i$ is the stiffness matrix, $\boldsymbol{F}^i$ is the generalized matrix with external load, $\boldsymbol{P}^i$ is the force array given by other components of the simulator, and $\boldsymbol{Q}^i$ is the inertial force matrix.

Considering the influence of elastic deformation, the moving platform has six independent DoF and the reference point of the moving platform changes from point C_4 to point C_4', the small deformation is expressed as $[\delta\alpha, \delta\beta, \delta\gamma, \delta x_C, \delta y_C, \delta z_C]$. The transformation matrix from the coordinate system $C_4' - x'y'z'$ to the coordinate system C_4-*xyz* is represented by $\Delta\boldsymbol{R}$. The elastic deformations are small and is based on Taylor expansion and Maclaurin in the formula, $\sin(\delta\alpha) \approx \delta\alpha$, and $\cos(\delta\alpha) \approx 1$.

In the absolute coordinate system,

$$\begin{bmatrix} x_{C_i'} \\ y_{C_i'} \\ z_{C_i'} \\ 1 \end{bmatrix} = \Delta\boldsymbol{R} \begin{bmatrix} x_{C_i} \\ y_{C_i} \\ z_{C_i} \\ 1 \end{bmatrix}, \Delta\boldsymbol{R} \approx \begin{bmatrix} 1 & -\delta\alpha & \delta\beta & \delta x_C \\ \delta\alpha & 1 & -\delta\gamma & \delta y_C \\ -\delta\beta & \delta\gamma & 1 & \delta z_C \\ 0 & 0 & 0 & 1 \end{bmatrix}. \tag{3}$$

The elastic displacement of the branched chain is as follows:

$$\begin{bmatrix} \Delta x_{C_i} \\ \Delta y_{C_i} \\ \Delta z_{C_i} \\ 1 \end{bmatrix} = \begin{bmatrix} x_{C_i'} \\ y_{C_i'} \\ z_{C_i'} \\ 1 \end{bmatrix} - \begin{bmatrix} x_{C_i} \\ y_{C_i} \\ z_{C_i} \\ 1 \end{bmatrix} = (\Delta\boldsymbol{R} - \boldsymbol{I}) \begin{bmatrix} x_{C_i} \\ y_{C_i} \\ z_{C_i} \\ 1 \end{bmatrix}. \tag{4}$$

The corresponding relationship between the changes of the node displacement and the six elastic changes of the moving platform is as follows:

$$\begin{bmatrix} \Delta x_{C_i} \\ \Delta y_{C_i} \\ \Delta z_{C_i} \end{bmatrix} = \begin{bmatrix} 1 & 0 & 0 & 0 & z_{C_i} & -y_{C_i} \\ 0 & 1 & 0 & -z_{C_i} & 0 & x_{C_i} \\ 0 & 0 & 1 & y_{C_i} & -x_{C_i} & 0 \end{bmatrix} \begin{bmatrix} \delta x_{C_o} \\ \delta y_{C_o} \\ \delta z_{C_o} \\ \delta\gamma \\ \delta\beta \\ \delta\alpha \end{bmatrix}, \tag{5}$$

where $[\Delta x_{Ci}, \Delta y_{Ci}, \Delta z_{Ci}]^{\mathrm{T}}$ is the component matrix of the displacement for the node C_i from nominal configuration to actual configuration along each axis of the absolute coordinate system.

According to Eq. (5), the kinematic constraints between the moving platform and the branched-chain $A_i P_i C_i$ expressed by $\boldsymbol{U}_{Ci}$ and $\boldsymbol{U}_0$ are as follows:

$$\boldsymbol{U}_{C_i} = \begin{bmatrix} 1 & 0 & 0 & 0 & z_{C_i} & -y_{C_i} \\ 0 & 1 & 0 & -z_{C_i} & 0 & x_{C_i} \\ 0 & 0 & 1 & y_{C_i} & -x_{C_i} & 0 \end{bmatrix} \boldsymbol{U}_0. \tag{6}$$

Equation (6) is abbreviated as

$$\boldsymbol{U}_{C_i} = \boldsymbol{J}_i \boldsymbol{U}_0, \tag{7}$$

https://doi.org/10.1017/S0263574721000151 Published online by Cambridge University Press

where $\boldsymbol{U}_{Ci}$ is the elastic displacement vector of the node C_i in branched-chain $A_iP_iC_i$, $\boldsymbol{U}_0$ is the deformation of the position and attitude for the moving platform caused by the elastic deformation of the branched chains, and $\boldsymbol{J}_i$ is the kinematic constraint matrix of the simulator.

Combined with Eq. (6), we can get:

$$\boldsymbol{\delta}_0 = \begin{bmatrix} \boldsymbol{R}_0 & 0 \\ 0 & \boldsymbol{R}_0 \end{bmatrix} \boldsymbol{U}_0, \tag{8}$$

where $\boldsymbol{\delta}_0 = [\delta_{01}, \delta_{02}, \delta_{03}, \delta_{04}, \delta_{05}, \delta_{06}]^{\mathrm{T}}$ is the deformation of the position and attitude for the moving platform in the coordinate system $C_4 - x'y'z'$, $\boldsymbol{U}_0 = [u_1, u_2, u_3, u_4, u_5, u_6]^{\mathrm{T}}$ is the deformation of the position and attitude for the moving platform in the coordinate system *O-XYZ*, and $\boldsymbol{R}_0$ is the transformation matrix of the coordinate system *O-XYZ* to the coordinate system $C_4 - x'y'z'$.

When the coupling effect between the nominal motion of the moving platform and the deformation caused by the elastic deformation of the branched chains is not considered, in the coordinate system *O-XYZ*, the velocity and the acceleration of the moving platform can be expressed as follows:

$$\begin{cases} \dot{\boldsymbol{u}}_0 = [\,\dot{x}_C + \dot{u}_1 \quad \dot{y}_C + \dot{u}_2 \quad \dot{z}_C + \dot{u}_3 \quad \dot{\gamma} + \dot{u}_4 \quad \dot{\beta} + \dot{u}_5 \quad \dot{\alpha} + \dot{u}_6\,]^{\mathrm{T}} \\ \ddot{\boldsymbol{u}}_0 = [\,\ddot{x}_C + \ddot{u}_1 \quad \ddot{y}_C + \ddot{u}_2 \quad \ddot{z}_C + \ddot{u}_3 \quad \ddot{\gamma} + \ddot{u}_4 \quad \ddot{\beta} + \ddot{u}_5 \quad \ddot{\alpha} + \ddot{u}_6\,]^{\mathrm{T}} \end{cases}. \tag{9}$$

Based on the Newton–Euler equation, the dynamic model of the moving platform is obtained as

$$\boldsymbol{M}_0\ddot{\boldsymbol{U}}_0 = \boldsymbol{f}_0 + \boldsymbol{F}_0 - \boldsymbol{M}_0\ddot{\boldsymbol{U}}_{0r}, \tag{10}$$

where $\boldsymbol{M}_0$ is the generalized mass matrix of the moving platform, $\boldsymbol{f}_0$ is the matrix of the resultant force and resultant moment of the branched chains acting on the moving platform, $\boldsymbol{F}_0$ is the matrix of external force and moment acting on the moving platform, and $\ddot{\boldsymbol{U}}_{0r}$ is the acceleration matrix of the moving platform.

Taking the generalized coordinates $\boldsymbol{U}_i^* = [u_{i1}, u_{i2}, \cdots, u_{i5}, u_{i6}, u_1, u_2, \cdots, u_6]^{\mathrm{T}}$, and based on Eq. (6), we can obtain:

$$\boldsymbol{U}_i = \boldsymbol{R}_i\boldsymbol{U}_i^*, \boldsymbol{R}_i = \begin{bmatrix} [\boldsymbol{I}_i]_{10\times10} & \boldsymbol{0} & \boldsymbol{0} \\ \boldsymbol{0} & \boldsymbol{0} & [\boldsymbol{J}_i]_{3\times6} \\ \boldsymbol{0} & [\boldsymbol{I}_i]_{3\times3} & \boldsymbol{0} \end{bmatrix}_{16\times19}. \tag{11}$$

Combining Eqs. (2) and (11), we can obtain:

$$\boldsymbol{M}^i\boldsymbol{R}_i\ddot{\boldsymbol{U}}_i^* + \boldsymbol{K}^i\boldsymbol{R}_i\boldsymbol{U}_i^* = \boldsymbol{F}^i + \boldsymbol{P}^i + \boldsymbol{Q}^i. \tag{12}$$

Both sides of Eq. (12) are left multiplied by $\boldsymbol{R}_i^{\mathrm{T}}$, and taking $\boldsymbol{M}_i = \boldsymbol{R}_i^{\mathrm{T}}\boldsymbol{K}^i\boldsymbol{R}_i$, $\boldsymbol{K}_i = \boldsymbol{R}_i^{\mathrm{T}}\boldsymbol{K}^i\boldsymbol{R}_i$, and $\boldsymbol{F}_i = \boldsymbol{R}_i^{\mathrm{T}}(\boldsymbol{F}^i + \boldsymbol{P}^i + \boldsymbol{Q}^i)$, Eq. (14) is rewritten as

$$\boldsymbol{M}_i\ddot{\boldsymbol{U}}_i^* + \boldsymbol{K}_i\boldsymbol{U}_i^* = \boldsymbol{F}_i, \tag{13}$$

where $\boldsymbol{M}_i = \begin{bmatrix} [\boldsymbol{M}_i^{11}]_{13\times13} & [\boldsymbol{M}_i^{12}]_{13\times6} \\ [\boldsymbol{M}_i^{21}]_{6\times13} & [\boldsymbol{M}_i^{22}]_{6\times6} \end{bmatrix}$, $\boldsymbol{K}_i = \begin{bmatrix} [\boldsymbol{K}_i^{11}]_{13\times13} & [\boldsymbol{K}_i^{12}]_{13\times6} \\ [\boldsymbol{K}_i^{21}]_{6\times13} & [\boldsymbol{K}_i^{22}]_{6\times6} \end{bmatrix}$, $\boldsymbol{U}_i^* = \begin{bmatrix} [\,\boldsymbol{U}_{0i}]_{13\times1} \\ [\boldsymbol{U}_0]_{6\times1} \end{bmatrix}$, $\boldsymbol{F}_i = \begin{bmatrix} [\,\boldsymbol{F}_i^1]_{13\times1} \\ [\boldsymbol{F}_i^2]_{6\times1} \end{bmatrix}$, and $\boldsymbol{U}_{0i} = [u_{i1}, u_{i2}, u_{i3}, u_{i4}, u_{i5}, u_{i6}, u_{i7}, u_{i8}, u_{i9}, u_{i10}, u_{i4}, u_{i5}, u_{i6}]^{\mathrm{T}}$.

Combining Eqs. (10) and (13), the undamped elastodynamic model of 3SPS+1PS parallel simulator is

$$\boldsymbol{M}\ddot{\boldsymbol{U}} + \boldsymbol{K}\boldsymbol{U} = \boldsymbol{F} - \boldsymbol{M}\ddot{\boldsymbol{U}}_r, \tag{14}$$

where $\boldsymbol{M}$ is the total mass matrix, $\boldsymbol{K}$ is the total stiffness matrix, $\boldsymbol{F}$ is the generalized force matrix, $\ddot{\boldsymbol{U}}_r$ is the acceleration matrix, $\boldsymbol{U}$ is the generalized coordinate matrix, and $\ddot{\boldsymbol{U}}$ is the second derivative matrix of generalized coordinates to time, that is the elastic acceleration matrix.

Considering the effect of damping in the elastodynamic analysis, and the viscous damping is directly proportional to the velocity of elastic deformation, the dynamic model of the simulator considering the effect of damping is as follows:

https://doi.org/10.1017/S0263574721000151 Published online by Cambridge University Press

$$\begin{cases} \boldsymbol{M}\ddot{\boldsymbol{U}} + \boldsymbol{C}\dot{\boldsymbol{U}} + \boldsymbol{K}\boldsymbol{U} = \boldsymbol{F} - \boldsymbol{M}\ddot{\boldsymbol{U}}_r \\ \boldsymbol{C} = \lambda_1 \boldsymbol{M} + \lambda_2 \boldsymbol{K} \end{cases}, \tag{15}$$

where $\dot{\boldsymbol{U}}$ is the first derivative of the generalized coordinates and is called elastic acceleration, $\boldsymbol{C} \in R^{61\times 61}$ is the damping matrix of the system,and λ_1 and λ_2 are Rayleigh damping scale coefficients.

Generally, when the elastic deformation is small, the relationship between deformation and load is linear. The component of deformation is a combination for the parallel simulator. The method to study the combined deformation is to calculate the stress and strain separately for each basic deformation, and then use these to obtain the stress and strain under the composite deformation of the system.

For the spatial circular section beam element, the bending stress at any point on the interface of the beam element can be expressed as follows:

$$\begin{cases} \boldsymbol{\sigma}_1(x,t) = Ez_D \dfrac{\partial^2 W_z(x,t)}{\partial x^2} \\ \boldsymbol{\sigma}_2(x,t) = Ey_D \dfrac{\partial^2 W_y(x,t)}{\partial x^2} \end{cases}, \tag{16}$$

$$\begin{cases} \dfrac{\partial^2 W_z(x,t)}{\partial x^2} = \left(\dfrac{\partial^2 \boldsymbol{N}_C}{\partial x^2}\right)^{\mathrm{T}} \boldsymbol{\delta}_e(t) = \ddot{n}_1\delta_{e3}(t) + \ddot{n}_2\delta_{e5}(t) + \ddot{n}_3\delta_{e8}(t) + \ddot{n}_4\delta_{e12}(t) + \ddot{n}_5\delta_{e14}(t) + \ddot{n}_6\delta_{e17}(t) \\ \dfrac{\partial^2 W_y(x,t)}{\partial x^2} = \left(\dfrac{\partial^2 \boldsymbol{N}_B}{\partial x^2}\right)^{\mathrm{T}} \boldsymbol{\delta}_e(t) = \ddot{n}_1\delta_{e2}(t) + \ddot{n}_2\delta_{e6}(t) + \ddot{n}_3\delta_{e9}(t) + \ddot{n}_4\delta_{e11}(t) + \ddot{n}_5\delta_{e15}(t) + \ddot{n}_6\delta_{e18}(t) \end{cases}$$

where $\boldsymbol{\delta}_e(t)$ is the elastic deformation vector of the element, $\boldsymbol{\delta}_{ei}(t)$ is the ith component in the elastic deformation, E is the elastic modulus of materials in tension and compression, y_D is the distance from any point on the section of element beam to z-axis, z_D is the distance from any point on the section of element beam to y-axis, $n = x/L$, L is the length of the branched chain, and $\ddot{n}_i$ is the second partial derivative of element configuration function to x.

The tensile and compressive stresses at any section of the beam element are as follows:

$$\sigma_3(x,t) = E\frac{\partial W_x(x,t)}{\partial x}. \tag{17}$$

$$\frac{\partial W_x(x,t)}{\partial x} = \left(\frac{\partial \boldsymbol{N}_A}{\partial x}\right)\boldsymbol{\delta}_e(t) = (\delta_{e10}(t) - \delta_{e1}(t))/L$$

For any moment of the simulator motion, the maximum normal stress on any section of beam element is

$$\sigma_{\max}(x,t) = \sigma_{1\max}(x,t) + \sigma_{2\max}(x,t) + \sigma_{3\max}(x,t). \tag{18}$$

The dynamic parameters of 3SPS+1PS parallel simulator are shown in Table I. According to ISO14242-1 for the standard of artificial hip joints, the motion curves of the simulator can be approximately simplified to trigonometric function curves, and the expression is as follows:

$$\begin{cases} \alpha = \dfrac{21.5\pi}{180}\cos(2\pi t) + \dfrac{3.5\pi}{180} \\ \beta = \dfrac{6\pi}{180}\cos(2\pi t + \pi) - \dfrac{4\pi}{180} \\ \gamma = \dfrac{5.5\pi}{180}\cos[2\pi(t - 0.21)] + \dfrac{1.5\pi}{180} \end{cases}, \tag{19}$$

where α, β, and γ are the attitude rotation angles of the moving platform for the parallel simulator, respectively.

Through the numerical simulation, the maximum stress of each branched chain of 3SPS+1PS parallel hip joint simulator is shown in Fig. 3(a), (b) and (c). In the process of the single motion cycle for the simulator, the maximum stress of each branched chain under Eq. (19) changes along with

https://doi.org/10.1017/S0263574721000151 Published online by Cambridge University Press

Table I. Dynamic parameters of 3SPS+1PS parallel hip joint simulator.

Parameter	**Value**	**Parameter**	**Value**
Material density ρ	7800 kg/m^3	Moving platform mass m_0	10 kg
Elasticity modulus E	2.1×10^{11}N/m^2	Moving platform Radius r	144 mm
Shear modulus G	7.85×10^{10}N/m^2	Base radius R	200 mm
Rayleigh coefficient λ_1	2×10^{-3}	Cylinder rod diameter d	30 mm
Rayleigh coefficient λ_2	3×10^{-4}	Cylinder body diameter D	40 mm

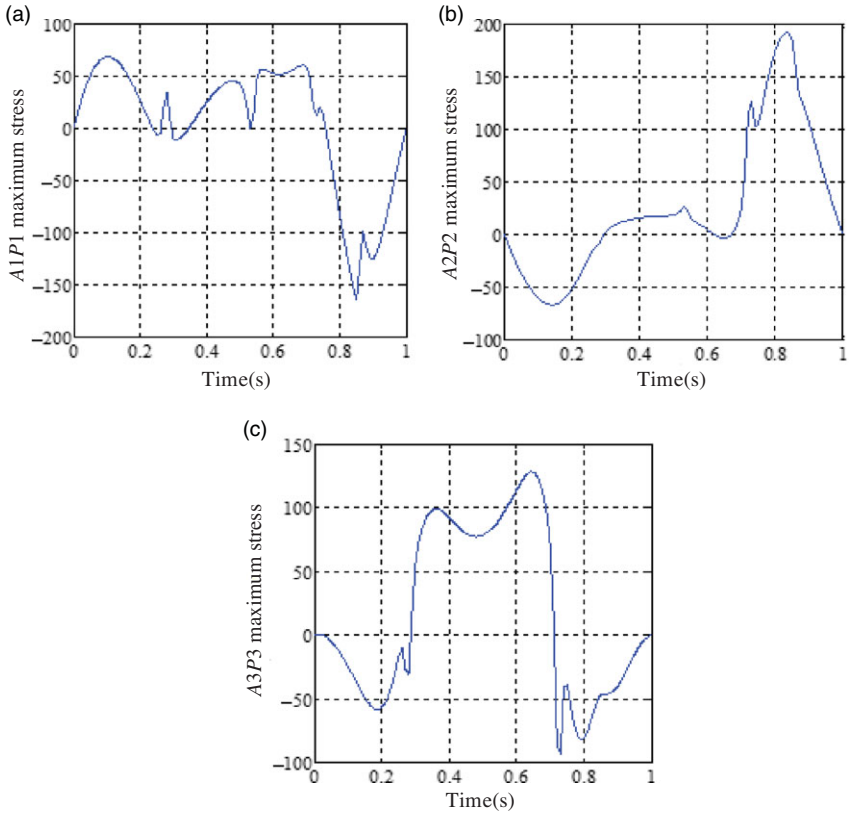

Fig. 3. Maximum stress of each branched chain for 3SPS+1PS parallel hip joint simulator. (a) Maximum stress of $A_1P_1C_1$. (b) Maximum stress of $A_2P_2C_2$. (c) Maximum stress of $A_3P_3C_3$.

time, and there are tensile stress and compressive stress at the same time. The maximum value of maximum stress for the branched-chain $A_2P_2C_2$ is the largest, and the maximum value of maximum stress for the branched-chain $A_3P_3C_3$ is the smallest. The result shows that the branched chains might have different fatigue life due to different stress.

3. Fatigue Life Analysis of 3SPS+1PS Parallel Simulator

3.1. Stress cycle counting method

The simplified process, the random and irregular stress-time course is transformed into a series of full-cycle or half-cycle processes with different amplitudes, is called the "Cycle counting method". The cycle counting method can simplify and shorten the stress-time course, and make it more convenient to deal with the results of stress tests and structural fatigue analysis. Rain-flow counting method is the cycle counting method with two parameters. It considers the influence of large stress amplitude and small stress amplitude on structural fatigue damage. However, the influence of the order of all stress amplitudes on fatigue life is not calculated.

https://doi.org/10.1017/S0263574721000151 Published online by Cambridge University Press

The Rain-flow counting method turns an actual stress-time course 90° and takes the vertical axis to represent time, and the horizontal axis to represent stress. The counting principle is as follows:

(1) The starting point of rain flow starts at the inner side of each peak (valley) value in turn;
(2) The rain flow falls at the next peak (valley) value until there is a larger (smaller) value on the opposite side than the peak (valley) value at the beginning;
(3) The rain flow stops when it comes to rain from the roof above;
(4) Take out all the full cycles and record their vibration ranges;
(5) Take out all the half cycles according to the positive and negative slopes, and record their vibration ranges;
(6) The half-cycle is counted according to the second stage of Rain-flow counting method.

3.2. Fatigue life analysis theory

For 3SPS+1PS parallel hip joint simulator, the fast speed, stress cycle, and complex geometric constraint relationship between the branched chains limit the elastic deformation of the branched chain. The fatigue of the branched chains for the parallel simulator is a type of high-cycle fatigue at low stress. The fatigue curve can be expressed by the following form:

$$(\sigma_{-1N})^m N_1 = (\sigma_{-1})^m N_0 = C, \tag{20}$$

where σ_{-1N} is the corresponding fatigue limit for the stress cycle is N, N_0 is the circular base, σ_{-1} is the endurance limit, and m and C are the material constants.

The dynamic stress amplitude of the branched chains calculated utilizing Kineto-Elasto Dynamics (KED) is unsteady, asymmetric, and variable, and so, it is required to be converted into a symmetric form as expressed in the formula below:

$$\sigma_{-1\mathrm{a}} = \sigma_{\mathrm{ra}} + \psi_\sigma \sigma_{\mathrm{rm}}, \tag{21}$$

where σ_{-1a} is the calculated symmetrical stress amplitude, σ_{ra} is the asymmetric stress amplitude, σ_{rm} is the average symmetrical stress amplitude, and ψ_σ is the reduction factor related to the materials.

The *S-N* curve can be utilized to estimate the number of cycles in which the material is destroyed under different stress levels. However, the *S-N* curve is not able to estimate the fatigue life directly when the branched chain is under two or more stress levels of the cyclic loading. In addition to the *S-N* curve, the Corten-Dolan cumulative damage theory can also estimate the fatigue life.

The Corten-Dolan fatigue cumulative damage theory is used to study the effect of alternating stress on the fatigue life experimentally and theoretically. Based on the theory, assuming that the damage starts at multiple locations on the specimen surface and each transformation cycle is called a stress cycle, then the stress characters can be determined based on the average value and amplitude of the stress. Finally, the development of fatigue damage is analyzed under the condition that stress σ_1 and σ_2 change alternately. Therefore, the calculation formula for the fatigue life can be expressed as

$$N_f = \frac{N_1}{\alpha + S^{1/\alpha}(1-\alpha)}, \tag{22}$$

where α is the ratio of the cycle numbers of the stress σ_1 to the total load cycles and N_1 is the cycle number till the fatigue damage occurs under single stress. The stress ratio $S = r_2/r_1$ is symmetrical in the stress cycle and r_1 and r_2 represent the damage coefficients corresponding to stress levels σ_1 and σ_2, respectively. S is related to the stress level, and $S^{1/a}$ can be replaced by $(\sigma_2/\sigma_1)^d$. The Eq. (22) can be re-expressed as

$$N_f = \frac{N_1}{\alpha + (\sigma_2/\sigma_1)^d(1-\alpha)}. \tag{23}$$

Equation (23) can be extended to multi-level loading:

$$N_f = \frac{N_1}{\sum_{j=1}^{k} \gamma_j \left(\frac{\sigma_j}{\sigma_{\max}}\right)^d}, \tag{24}$$

https://doi.org/10.1017/S0263574721000151 Published online by Cambridge University Press

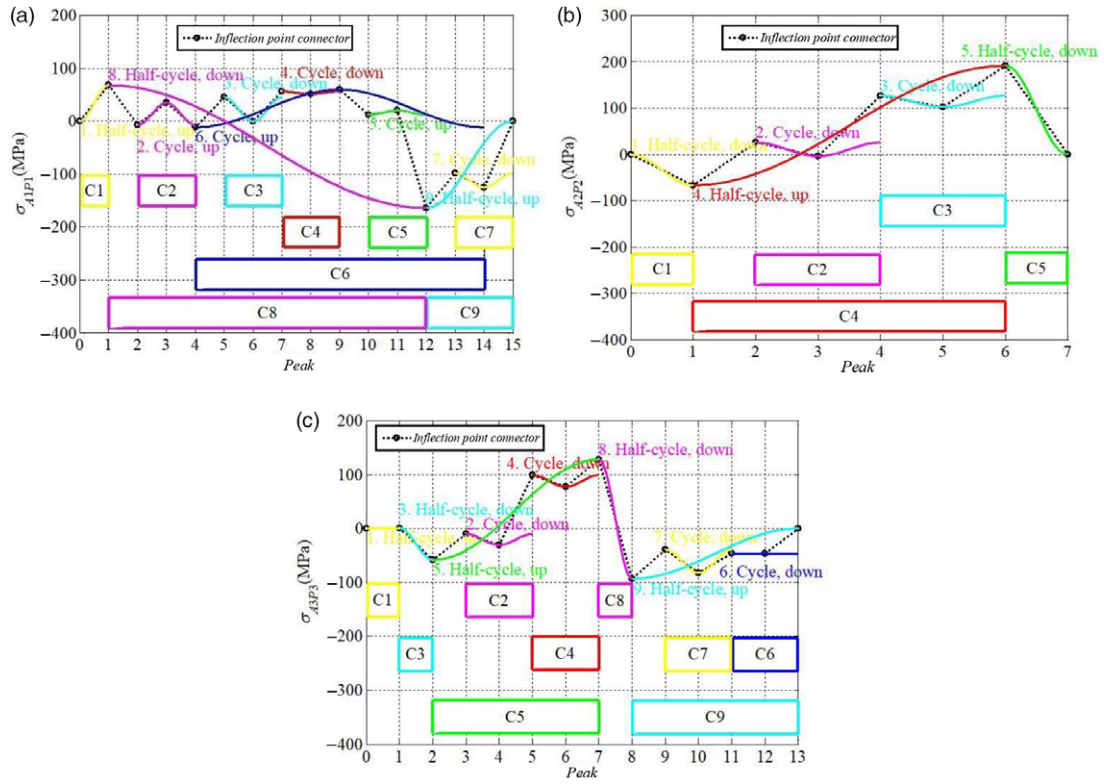

Fig. 4. Number of cycles in the stress-time course of branched chains. (a) Branched-chain $A_1P_1C_1$. (b) Branched-chain $A_2P_2C_2$. (c) Branched-chain $A_3P_3C_3$.

where N_f is the cycle numbers until the material is destroyed, N_1 is the cycle numbers under maximum stress $\sigma_{\max}$, $\sigma_{\max}$ is the maximum alternation stress under the multistage load, γ_j is the percentage of circulation under alternating stress $\sigma_j (j = 1, 2, 3, \ldots,)$, k is the number of the cycle, and d is a material constant.

3.3. Fatigue life analyses of branched chains

Through the analysis of the stress variation for three branched chains, we conclude that the root of each branched chain is relatively weak and the value of the dynamic stress is also the largest. The statistics of the stress cycling of each branched chain at all the levels are collected by Rain-flow counting method, and the results are shown in Fig. 4(a), (b) and (c).

The stress amplitude is the main factor that causes the fatigue cumulative damage, and Rain-flow counting method is utilized to filter out all the stress cycles from the branched-chain stress-time course. Minimum stress $\sigma_{\min}$, maximum stress $\sigma_{\max}$, average stress $\sigma_{\rm rm}$, stress amplitude $\sigma_{\rm ra}$, and symmetrical cyclic stress σ_{-1a} converted among all the stress spectra of the three driven branched chains are listed in Tables II–V.

The fatigue lives of the branched chains of the 3SPS+1PS parallel simulator can be estimated according to the data in Tables II– IV. The number of cycles until the branched chain is destroyed under the maximum stress can be determined by Eq. (20), and Eq. (24) is utilized to evaluate the fatigue life of branched chain under the KED stress spectrum.

In Eqs. (20) and (24), taking the parameters $\sigma_0 = 110$ Mpa, $\sigma_{\max} = 164.1$ MPa, $m = 9$, and $d = 4.8$, the fatigue life of the branched-chain $A_1P_1C_1$ can be calculated as follows:

$$N_1 = \left(\frac{\sigma_0}{\sigma_{\max}}\right)^m N_0 = 2.732 \times 10^5.$$

$$N_{f1} = \frac{N_1}{\sum_{j=1}^{k} \gamma_j \left(\frac{\sigma_j}{\sigma_{\max}}\right)^d} = 5.4868 \times 10^6 \text{cycles}.$$

https://doi.org/10.1017/S0263574721000151 Published online by Cambridge University Press

Table II. Stress cycles at all stress spectra of branched-chain $A_1P_1C_1$.

Cycle	σ_{min}(MPa)	σ_{max}(MPa)	σ_{rm}(MPa)	σ_{ra}(MPa)	σ_{-1a}(MPa)	Full/Half-cycle
C1	0.06	68.14	34.10	34.04	51.09	0.5
C2	−11.73	34.77	11.52	23.25	29.01	1
C3	−0.51	45.29	22.39	22.90	34.10	1
C4	51.33	56.48	53.91	2.58	29.54	1
C5	12.05	20.50	16.28	4.23	12.37	1
C6	−11.73	60.00	24.14	35.87	47.94	1
C7	−125.27	−98.27	−111.77	13.50	−42.39	1
C8	−164.10	58.14	−47.98	116.12	92.13	0.5
C9	−164.10	0.06	−82.02	82.08	41.07	0.5

Table III. Stress cycles at all stress spectra of branched-chain $A_2P_2C_2$.

Cycle	σ_{min}(MPa)	σ_{max}(MPa)	σ_{rm}(MPa)	σ_{ra}(MPa)	σ_{-1a}(MPa)	Full/Half-cycle
C1	−66.69	0.03	−33.33	33.36	16.70	0.5
C2	−0.17	25.94	12.89	13.06	19.51	1
C3	102.32	130.43	116.39	14.06	72.26	1
C4	−66.69	191.30	62.30	129.00	160.15	0.5
C5	0.03	191.30	95.67	95.64	143.48	0.5

Table IV. Stress cycles at all stress spectra of branched-chain $A_3P_3C_3$.

Cycle	σ_{min}(MPa)	σ_{max}(MPa)	σ_{rm}(MPa)	σ_{ra}(MPa)	σ_{-1a}(MPa)	Full/Half-cycle
C1	0.05	0.56	0.31	0.26	0.42	0.5
C2	−30.58	−10.05	−20.32	10.27	0.11	1
C3	−58.37	0.56	−28.91	29.47	15.02	0.5
C4	77.33	99.12	88.23	10.90	55.02	1
C5	−58.37	128.11	34.87	93.24	110.68	0.5
C6	−46.52	−46.16	−46.34	0.18	−22.99	1
C7	−82.18	−38.98	−60.58	21.60	−8.69	1
C8	−82.18	128.10	22.96	105.14	116.62	0.5
C9	−82.18	0.05	−41.07	41.12	20.59	0.5

Similarly, according to Tables III and IV, the fatigue life of the branched-chain $A_2P_2C_2$ and the branched-chain $A_3P_3C_3$ can be calculated as

$$N_{f2} = 4.1315 \times 10^6 \text{cycles}, \; N_{f3} = 7.3556 \times 10^6 \text{cycles}.$$

For the 3SPS+1PS parallel hip joint simulator, the time of a motion cycle is 1s. When the simulator is used for continuous tests of artificial hip joints, the fatigue lives of branched chains can be converted into $N_{f1} \approx 63.50$ days, $N_{f2} \approx 47.82$ days, and $N_{f3} \approx 85.13$ days when the branched chains never stop moving. The results show that the fatigue life of the branched chain is different. The branched-chain $A_3P_3C_3$ has the longest fatigue life, and the fatigue life of the branched-chain $A_2P_2C_2$ is the weakest. Therefore, it is necessary to replace the branched chain or adjust the motion parameters of the simulator according to the fatigue life analysis of the branched chains.

Combined with Fig. 3, there is a corresponding relationship between the fatigue life and the maximum stress for the branched chain. In a motion cycle, the smaller the maximum stress on the branched chain, the longer the fatigue life. The calculation indicates that branched-chain $A_2P_2C_2$ is weaker than the other branched-chains of the simulator. Therefore, it will enter the stage of fatigue failure earlier and result in a system crash. During the design for the parallel simulator, the parameters of the rods can be adjusted appropriately to reduce the dynamic stress and prolong the lives for the rods to equilibrate, thereby, enhancing the dynamics performance.

https://doi.org/10.1017/S0263574721000151 Published online by Cambridge University Press

Table V. Distribution of the random variables of 3SPS+1PS parallel hip joint simulator.

Random variable	**Distribution**	**Average**	**Variance**
Elasticity modulus E (N/m^2)	Normal distribution	2.1×10^{11}	2.1×10^{10}
Shear modulus G (N/m^2)	Normal distribution	7.85×10^{10}	7.85×10^{9}
Material density ρ (kg/m^3)	Normal distribution	7800	780
Cylinder rod diameter d (m)	Uniform distribution	0.0300	0.0030
Cylinder rod length l_u (m)	Uniform distribution	0.2800	0.0280
Cylinder diameter D (m)	Uniform distribution	0.0400	0.0040
Cylinder length l_d (m)	Uniform distribution	0.4000	0.0400
Moving platform radius e (m)	Uniform distribution	0.1440	0.0144
Moving platform mass m_0 (kg)	Uniform distribution	10	1.0000
Middle branched-chain height H (m)	Uniform distribution	0.6900	0.0690

To verify the correctness of the fatigue life model for the branched chains, the same structural parameters model as the theoretical analysis is established with ANSYS. The minimum values of fatigue lives for branched chains in FEA are $N_{FEA\_f1} = 4.0363 \times 10^6$ cycles, $N_{FEA\_f2} = 2.8508 \times 10^6$ cycles, and $N_{FEA\_f3} = 6.1472 \times 10^6$ cycles. Compared with N_{f1}, N_{f2}, and N_{f3}, the results of FEA are basically consistent with the theoretical calculation, and it also shows the fatigue life model for the simulator is effective. Besides, the FEA values are slightly less than the theoretical calculation, this is because the stress of the branched chain is mainly considered in the theoretical calculation, while the influence of other factors on the fatigue life is ignored.

4. Fatigue Reliability Analysis of 3SPS+1PS Parallel Simulator

4.1. Fatigue reliability analysis method

The purpose of fatigue reliability analysis is to ensure that 3SPS+1PS parallel hip joint simulator can operate within the design life as well as avoid early failure because of the materials fatigue cumulative damage. The reliable characteristics include the reliability, accumulated invalidation probability (or unreliability), average life, reliable life, and failure rate. These indicators reflect the general reliability level of a simulator. Combined with cumulative fatigue damage or crack growth theory, the model considers the fatigue life as the parameter to analyze the fatigue reliability. The safety margin equation for the fatigue life model can be expressed as

$$M_N = N_0 - N, \tag{25}$$

where N_0 is the design life and N is the fatigue life of the components under loading.

Design life N_0 can be expressed as

$$P_r = P\left\{N_0 - N \geq 0\right\}. \tag{26}$$

4.2. Reliability analysis based on the fatigue life model

The dynamic stress of branched chains is a type of function that is related to the structural parameters and some physical constants. Each random parameter of the stress analytic function is set as $X_j (j = 1, 2, \ldots, n)$. It is assumed that the structural parameters of the mechanism follow a normal distribution, and all the physical constants are considered to follow a uniform distribution. The parameters are listed in Table V.

The Monte Carlo model is established by MATLAB, and the simulation times are 1000. Using a mathematical method, we obtain n random arrays Z_{js} that obey a uniform distribution or normal distribution in the range of the parameters. Subscript j is the label of random parameter X_j and s represents the number of simulations. Substituting the values of the random parameters (X_{1s}, X_{2s}, $\ldots$, X_{ns}) obtained from the simulations into Eq. (18), the corresponding dynamic stress sample of each branched chain can be derived. After repeated simulation for m times, m dynamic stress samples of each branched chain can be obtained. According to the fatigue life analysis of the branched chains, a group of the fatigue life distribution of each branched chain is obtained. Next, utilizing the samples for the statistical analysis, the distribution histogram of the fatigue life is plotted and fitted to the

https://doi.org/10.1017/S0263574721000151 Published online by Cambridge University Press

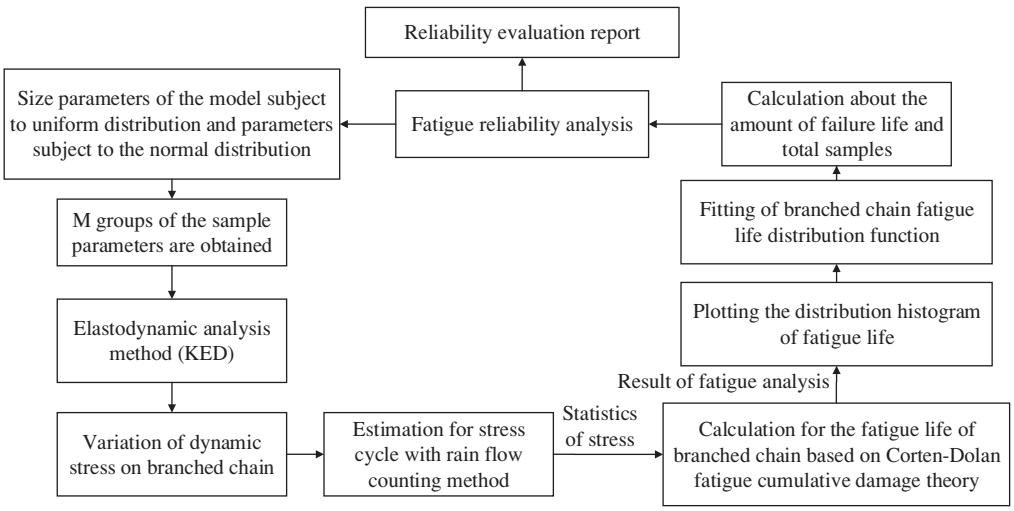

Fig. 5. Flow diagram of the reliability analysis for the fatigue life.

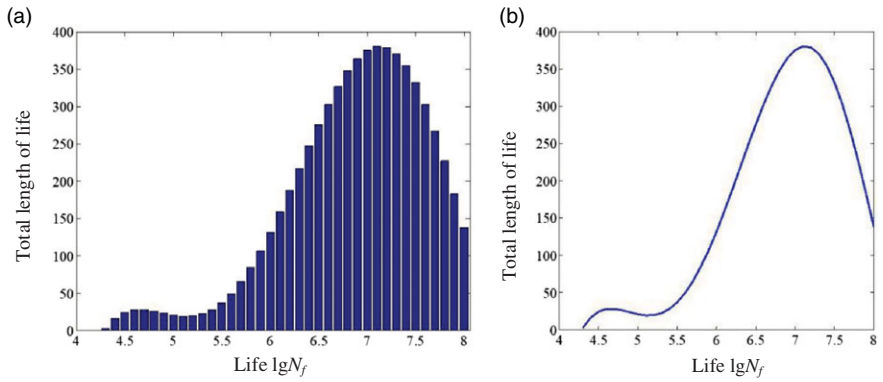

Fig. 6. Logarithm life of the simulator. (a) Distribution histogram. (b) Fitting function.

fatigue life distribution function. Finally, the reliability is calculated and evaluated based on the fatigue life distribution function. The process is shown in Fig. 5.

The calculated dynamic stresses exhibit a trend that the dynamic stress of the branched-chain $A_1P_1C_1$ and $A_3P_3C_3$ is higher than that of the branched-chain $A_2P_2C_2$ under the same structural parameters. The fatigue life of each branched chain displays a similar variation and the branched-chain $A_2P_2C_2$ has the minimum fatigue life. The damage of a single branched chain will cause the failure of the whole simulator; therefore, this study only considers the fatigue reliability of the branched-chain $A_2P_2C_2$. The distribution histogram for the fatigue life of the branched-chain $A_2P_2C_2$ is shown in Fig. 6(a) and the fitting function of the logarithm life is shown in Fig. 6(b).

If logarithm life lg N_f is represented as κ, the fitting function of the logarithm life based on the fatigue life distribution histogram is expressed as

$$F(\kappa) = 16.009\kappa^6 - 519.519\kappa^5 + 6906.016\kappa^4 - 48152.491\kappa^3 + 185880.467\kappa^2 - 376978.357\kappa + 314073.330 \quad . \tag{27}$$

3SPS+1PS parallel simulator needs to satisfy that the tests are no less than 3×10^6 times (it is equivalent to the amount of exercise of the artificial hip joint in a patient for 2–3 years). When the simulator runs for a duration of 3×10^6 s, the corresponding logarithm life is 6.47. Hence, the simulator is considered fatigue failure when the calculated logarithm life is less than 6.47 and the range of the fatigue failure life is $4 \leq \kappa \leq 6.47$, as shown in Fig. 6.

https://doi.org/10.1017/S0263574721000151 Published online by Cambridge University Press

Table VI. Fatigue life of 3SPS+1PS parallel simulator with different structural parameters.

Structural parameters (mm)	Fatigue life of branched chains (cycles) $A_1 P_1 C_1$	$A_2 P_2 C_2$	$A_3 P_3 C_3$	Reliability
Cylinder rod diameter $d = 30.0$ Cylinder body diameter $D = 40.0$	5.4868×10^6	4.1315×10^6	7.3556×10^6	0.6426
Cylinder rod diameter $d = 30.0$ Cylinder body diameter $D = 41.5$	6.0588×10^6	5.2789×10^6	8.4731×10^6	0.6724
Cylinder rod diameter $d = 31.5$ Cylinder body diameter $D = 40.0$	7.0458×10^6	6.0841×10^6	9.7843×10^6	0.7095

For the discretization of the fatigue life, a fatigue life value κ_r is selected in the interval 0.01, and the value is substituted into Eq. (22) to obtain the corresponding number of the samples. The number of samples $F(\kappa_r)$ corresponding to each life value κ_r is summed. The number of samples corresponding to the failure life of the simulator is

$$\begin{aligned} F(4 \le \kappa_r \le 6.47) &= \sum_{\kappa_r=1}^{\kappa_r=247} F(\kappa_r) \\ &= 16.009\kappa_r^6 - 519.519\kappa_r^5 + 6906.016\kappa_r^4 - 48152.49\kappa_r^3 \cdot \\ &\quad + 185880.467\kappa_r^2 - 376978.357\kappa_r + 314073.330 \end{aligned} \tag{28}$$

The calculated samples of the fatigue life in the range $4 \le \kappa \le 6.47$ are $F(4 \le \kappa \le 6.47) = 33695$ when the length of the calculation step is 0.01.

The samples of the fatigue life in the entire sample interval $4 \le \kappa \le 8$ are as follows:

$$F(4 \le \kappa \le 8) = \sum_{\kappa_r=1}^{\kappa_r=400} F(\kappa_r) = 94267. \tag{29}$$

The failure probability of 3SPS+1PS parallel simulator is

$$P(\kappa \le 6.47) = 1 - \frac{F(4 \le \kappa \le 6.47)}{F(4 \le \kappa \le 8)} = 1 - \frac{33695}{94267} = 0.6426. \tag{30}$$

4.3. Effect of branched-chain structural parameters on the reliability

Different structure parameters of the branched chains are selected for studying the effect of the structural parameters on the fatigue reliability. The values, fatigue lives, and fatigue reliability under different parameters are shown in Table VI.

The results indicate that the fatigue life and reliability of the branched chains can be increased to a certain degree by increasing the diameter of the cylinder rod and cylinder body. When the cylinder body diameter increases from 40.0 to 41.5 mm, the fatigue life of the branched-chain $A_1P_1C_1$, $A_2P_2C_2$, and $A_3P_3C_3$ increases by 10.4%, 27.7%, and 15.2%, respectively, and the fatigue reliability increases by 4.6%. When the cylinder rod diameter increases from 30.0 to 31.5 mm, the fatigue life by increases by 28.4%, 47.3%, and 33.0%, respectively, and the fatigue reliability increases by 10.4%. It is noteworthy that the effect on the fatigue life of increasing the diameter of the upper branched chain (the cylinder rod diameter) is higher, and increasing the cylinder rod diameter can significantly improve the fatigue reliability.

Furthermore, three branched chains of 3SPS+1PS parallel simulator have the same structural parameters, and the structure of the simulator is completely symmetrical in space. It is effective to balance the difference of fatigue life between branched chains by changing the initial motion parameters among the three chains. After the parallel simulator has been running for a while, the motion parameters of branched-chain $A_1P_1C_1$ and $A_3P_3C_3$ can be regularly exchanged to balance the fatigue life gap between branched chains.

https://doi.org/10.1017/S0263574721000151 Published online by Cambridge University Press

5. Conclusion

For 3SPS+1PS parallel hip joint simulator, based on the Corten-Dolan fatigue cumulative damage theory and the Rain-flow counting method, the fatigue lives of branched-chains $A_1P_1C_1$, $A_2P_2C_2$, and $A_3P_3C_3$ are 5.4868×10^6 cycles, 4.1315×10^6 cycles, and 7.3556×10^6 cycles, respectively. The dynamic stress of branched-chain $A_2P_2C_2$ is the highest and its fatigue life is the shortest. Therefore, it is the weakest part of the simulator.

Setting the structure parameters as random variables, the subsamples of random parameters are obtained by random sampling and the corresponding dynamic stress samples are obtained by elasto-dynamics. The fatigue reliability of the branched-chain $A_2P_2C_2$ is used to represent the reliability of the simulator. The fatigue life samples can be obtained by the fatigue life analysis, and based on the fatigue life fitting function, the reliability of the parallel simulator is 0.6426.

The study indicates that an appropriate increase in the cylinder rod diameter can result in a significant improvement of the fatigue life and reliability. This paper also provides a theoretical basis for the exchange of initial motion parameters to balance the fatigue life gap between branched chains.

Acknowledgments

Financial support for this work, provided by the Priority Academic Program Development of Jiangsu Higher Education Institutions and the National Natural Science Foundation of China (Grant No. 91648105), is gratefully acknowledged.

Conflict of Interest

The authors declare that they have no competing interests.

References

1. N. Lobontiu, "Modeling and design of planar parallel-connection flexible hinges for in- and out-of-plane mechanism applications," *Precis. Eng.* **42**(1), 113–132 (2015).
2. Y. Lu, Y. Liu, L. Zhang and N. Ye, "Dynamics analysis of a novel 5-DoF parallel manipulator with couple-constrained wrench," *Robotica* **36**(10), 1421–1435 (2018).
3. M. Zhou, Q. Yu, K. Huang, S. Mahov, A. Eslami, M. Maier, C. Lohmann, N. Navab, D. Zapp, A. Knoll and M. Nasseri, "Towards robotic-assisted subretinal injection: A hybrid parallel–serial robot system design and preliminary evaluation," *IEEE T. Ind. Electron.* **67**(8), 6617–6628 (2020).
4. H. Qu and S. Guo, "Kinematics analysis of a novel planar parallel manipulator with kinematic redundancy," *J. Mech. Sci. Technol.* **31**(4), 1927–1935 (2017).
5. G. Chen, W. Yu, Q. Li and H. Wang, "Dynamic modeling and performance analysis of the 3-PRRU 1T2R parallel manipulator without parasitic motion," *Nonlinear Dynam.* **90**(1), 339–353 (2017).
6. G. Cheng, Y. Li, L. Feng, X. Shan and J. Yang, "Configuration bifurcation and self-motion analysis of 3SPS+1PS bionic parallel test platform for hip joint simulator," *Mech. Mach. Theory* **86**, 62–72 (2015).
7. L. Xu, G. Chen, W. Ye and Q. Li, "Design, analysis and optimization of Hex4, a new 2R1T overconstrained parallel manipulator with actuation redundancy," *Robotica* **37**(2), 358–377 (2019).
8. S. Mohan, "Error analysis and control scheme for the error correction in trajectory-tracking of a planar 2PRP-PPR parallel manipulator," *Mechatronics* **46**, 70–83 (2017).
9. X. Shan and G. Cheng, "Structural error identification and kinematic accuracy analysis of a 2(3PUS+S) parallel manipulator," *Measurement* **140**, 22–28 (2019).
10. X. Sun, Y. Zhang and D. Shi, "Dynamics simulation and fatigue life study of the drive system of rack and pinion climbing vertical shiplift," *Appl. Mech. Mater.* **456**, 155–158 (2013).
11. S. Nie, Y. Li, G. Shuai, S. Tao and F. Xi, "Modeling and simulation for fatigue life analysis of robots with flexible joints under percussive impact forces," *Robot. Comput. Integr. Manuf.* **37**, 292–301 (2016).
12. S. Guo, Y. He, L. Shi, S. Pan, K. Tang, R. Xiao and P. Guo, "Modal and fatigue analysis of critical components of an amphibious spherical robot," *Microsyst Technol.* **23**, 2233–2247 (2017).
13. C. Liu, Z. Lu, Y. Xu and Z. Yue, "Reliability analysis for low cycle fatigue life of the aeronautical engine turbine disc structure under random environment," *Mat. Sci. Eng. A-Struct.* **395**(1–2), 218–225 (2005).
14. Y. Yan, "Load characteristic analysis and fatigue reliability prediction of wind turbine gear transmission system," *Int. J. Fatigue* **130**, 105259.1–105259.9 (2020).
15. M. Kassner, "Fatigue strength analysis of a welded railway vehicle structure by different methods," *Int. J. Fatigue* **34**(1), 103–111 (2012).
16. Y. Cai, Y. Zhao, X. Ma and Z. Yang, "An extended model for fatigue life prediction and acceleration considering load frequency effect," *IEEE Access* **6**, 21064–21074 (2018).
17. Y. Kim, K. Lee, H. Li, C. Seok, J. Koo, S. Kwon and Y. Cho, "Fatigue life prediction method for contact wire using maximum local stress," *J. Mech. Sci. Technol.* **29**(1), 67–70 (2015).

18. H. Gao, H. Huang, Z. Lv, F. Zuo and H. Wang, "An improved Corten-Dolan's model based on damage and stress state effects," *J. Mech. Sci. Technol.* **29**(8), 3215–3223 (2015).
19. Q. Liu, Y. Gao, Y. Li and Q. Xue, "Fatigue life prediction based on a novel improved version of the Corten-Dolan model considering load interaction effect," *Eng. Struct.* **221**, 111036 (2020).
20. H. Cheng, J. Tao, X. Chen and Y. Jiang, "A method for estimating rainflow fatigue damage of narrowband non-Gaussian random loadings," *P. I. Mech. Eng. C-J. Mec*. **228**(14), 2459–2468 (2014).
21. C. Chen, Z. Yang, J. He, H. Tian, S. Li and D. Wang, "Load spectrum generation of machining center based on rainflow counting method," *J. Vibroeng.* **19**(8), 5767–5779 (2017).

https://doi.org/10.1017/S0263574721000151 Published online by Cambridge University Press